11(2014) 131 - 141

Latin American Journal of Solids and Structures
www.lajss.org

# Dynamic compressive behavior of recycled aggregate concrete based on split Hopkinson pressure bar tests

**Abstract**

This paper presents the experimental results of recycled aggregate concrete (RAC) specimens prepared with five different amount of recycled coarse aggregate (RCA) [i.e. 0, 25%, 50%, 75% and 100%] subjected to compressive loading based on split Hopkinson pressure bar tests. Strain-rate effects on dynamic compressive strength and critical strain of recycled aggregate concrete were studied. Results show that impact properties of recycled aggregate concrete exhibit strong strain-rate dependency, and increase approximately linearly with strain-rate. The transition point from low strain-rate sensitivity to high sensitivity decreases with the increase of matrix strength.

**Keywords**

Recycled coarse aggregate (RCA); recycled aggregate concrete (RAC); split Hopkinson pressure bar tests; compressive strength; strain-rate.

**Yubin Lu** [*, a]
**Xing Chen** [b]
**Xiao Teng** [b]
**Shu Zhang** [b]

[a] Key Laboratory of Testing Technology for Manufacturing Process (Ministry of Education), Southwest University of Science and Technology, Mianyang 621010, Sichuan, PR China,
[b] School of Manufacturing Science and Technology, Southwest University of Science and Technology, Mianyang, 621010

Received in 10 Jan 2013
In revised form 11 Apr 2013

[*]Author email: yubinluzju@hotmail.com

## 1 INTRODUCTION

The amount of construction and demolition waste (C&DW) has increased enormously over the last decade in the entire world. The recycling of waste concrete is beneficial and necessary for the environmental preservation and effective utilization of natural resources. The use of recycled coarse aggregate (RCA) obtained from C&DW in new concrete is a solution for effective utilization of construction and demolition waste.

In practice, there are many incidents in which the structures undergo impact or explosion loading. The behavior of concrete structures subjected to dynamic loading is different from that under quasi static loading. Due to short duration of loading, the strain-rate of material is significantly higher than that under quasi static loading conditions. Therefore, the present paper focuses on the dynamic compressive behavior of recycled aggregate concrete (RAC) specimens prepared with different amount of RCA under dynamic loading based on split Hopkinson pressure bar (SHPB) tests.

Many researchers have studied the dynamic compressive behavior of plain, composite and reinforced concrete specimens with natural coarse aggregates (NCA) based on SHPB tests. For example, Li and Xu (2009) studied the impact mechanical properties of basalt fiber reinforced geopolymeric

concrete based on a SHPB system; Rong et al. (2010) investigated the dynamic compression behavior of ultra-high performance cement based composites; Wang et al. (2008) obtained the stress–strain relationship of steel fiber-reinforced concrete under dynamic compression based on SHPB. For RAC, Chakradhara Rao et al. (2011) have studied its behavior under low velocity drop weight impact load. But no attempts have been made on the behavior of RAC specimens based on SHPB tests.

In this paper, the impact compression experiment is described in detail, including the preparation of RAC specimens and the SHPB test, in Section 2. Results of stress versus strain curves, failure patterns, strength, deformation and energy absorption are presented and discussed in Section 3, followed by conclusions in Section 4.

## 2 EXPERIMENTS

### 2.1 Materials

Raw materials used for RAC specimens are (1)RCA taken from waste concrete of a Mianyang road, the design strength of this waste concrete is unclear, and the waste concrete is broken by a jaw crusher, graded and cleaned to RCA of diameters from 10 to 20 mm; (2)NCA, natural cobbles of diameters from 10 to 20 mm; (3)ordinary Portland cement of 42.5 grade; (4)fine aggregates, natural river sand of continuous grading with fineness modulus of 2.28; and (5)Mianyang tap water.

Concrete mix proportions largely influence the mechanical properties of concrete. To ensure the flowability during concreting and the strength after molding of RAC, the mix proportions of RAC specimens used in this study are cement: water: fine aggregate: coarse aggregate=1:0.477:1.465:3.418, where coarse aggregates include NCA and RCA. According to the difference of replacement ratios of RCA, there are five different types of specimens, as shown in Table 1. PC-0 stands ordinary concrete specimens, and RC-25, RC-50, RC-75 and RC-100 stand RAC specimens with RCA replacement ratio of 25%, 50%, 75% and 100%, respectively.

Table 1 The mix proportions of RAC test specimens.

| Mix designation | Cement | Water | Sand | NCA | RCA | Replacement ratio/% |
|---|---|---|---|---|---|---|
| PC-0 | 1 | 0.477 | 1.465 | 3.418 | 0 | 0 |
| RC-25 | 1 | 0.477 | 1.465 | 2.564 | 0.854 | 25 |
| RC-50 | 1 | 0.477 | 1.465 | 1.709 | 1.709 | 50 |
| RC-75 | 1 | 0.477 | 1.465 | 0.854 | 2.564 | 75 |
| RC-100 | 1 | 0.477 | 1.465 | 0 | 3.418 | 100 |

### 2.2 SHPB tests

Dynamic compression tests of RAC are performed on 100-mm-diameter SHPB setup with $\phi 100 \times 50$ mm cylinder specimens. The SHPB setup is shown in Figure 1. The length of the projectile, incident and transmission bar is 0.5, 4.5 and 2.5 m, respectively. The distance from the strain gauges on the incident bar and transmission bar and the interface of incident bar/specimen or speci-

men/transmission bar is 2.5 m and 0.5 m. The projectile, incident and transmission bar are made of 48CrMoA and have Young's modulus of 210 GPa, density of 7850 kg/m$^3$, Poisson's ratio of 0.25-0.3, theoretical elastic wave velocity of 5172 m/s, and measured elastic wave velocity of 5200 m/s. The projectile bar is accelerated by the use of air pressure, and the projectile striking velocity is measured by laser velocimeter with the light distance of 0.1 m.

Ravichandran et al. (1994) proved that some time is needed for the specimen to achieve stress equilibrium state after it is first loaded, and this time is approximately $4\tau_s$ (where $\tau_s$ is the transit time for the leading edge of the stress pulse traveling through the specimen). Pulse shaping technique (Lu and Li, 2010) can prolong the rise time of incident pulse, so that specimens have enough time to obtain stress equilibrium. Besides, it can smooth waveforms and eliminate waveform oscillations. In this study, for striking velocities <6 m/s, 6-10 m/s and 10-12 m/s, three different kinds of pulse shapers are used, i.e., pasteboard of 0.67 mm thickness and 54.27 mm diameter, H62 brass of 1 mm thickness and 20 mm diameter, and H62 brass of 1 mm thickness and 30 mm diameter pulse shapers were respectively designed to improve incident waveforms. The pulse shapers are shown in Figure 2.



(a) Overall setup



Before impact



After impact

(b) Specimen, incident and transmitted bars

Figure 1 The 100-mm-diameter SHPB apparatus.

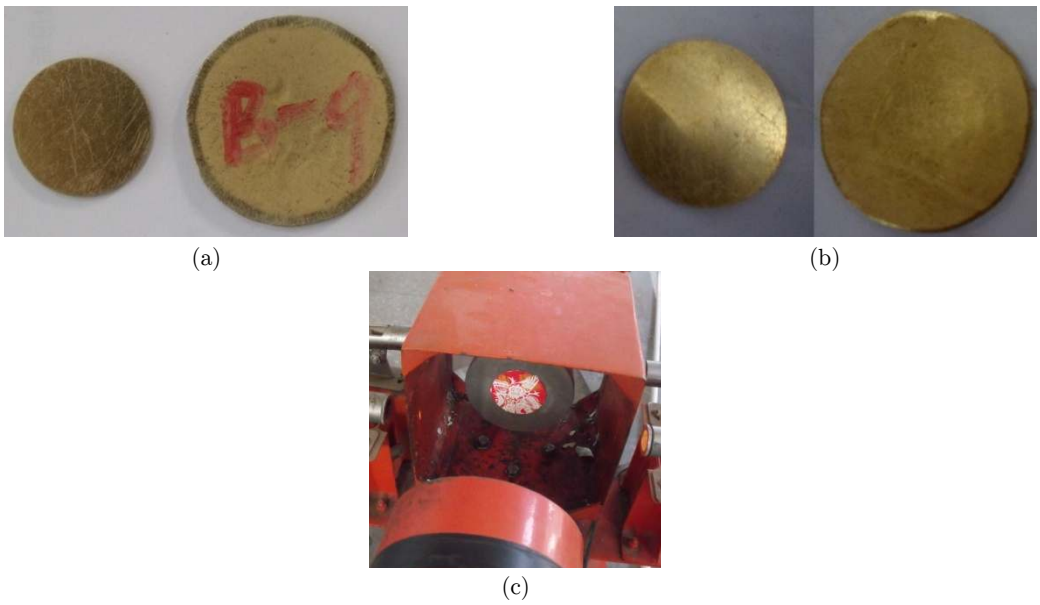

Figure 2 Original and deformed H62 brass pulse shaper photos for (a) $\phi$ 20 × 1 mm and (b) $\phi$ 30 × 1 mm, (c) pasteboard pulse shaper attached to the incident bar.

Figure 3 presents the comparison of shaped incident pulses by different pulse shapers. After using pulse shapers, the total duration of incident pulse is 433.5–514.5 μs and the rise time is up to 124.5–204.0 μs. Except the use of brass pulse shaper with 20 mm in diameter when the striking velocity is 11.0 m/s (the rise time is 124.5 μs), other pulse shapers provide sufficient time for the specimen to achieve stress equilibrium state. However, for low striking velocity (about 5 m/s), the shaped effect of pasteboard is better than that of brass with 10 mm in diameter. Figure 4 shows the typical incident, reflected and transmitted waveforms of a natural aggregate concrete (NAC) specimen shaped by a brass pulse with diameter of 20 mm. It shows that the dispersion of strain pulse during SHPB test is eliminated by the use of this pulse shaper.

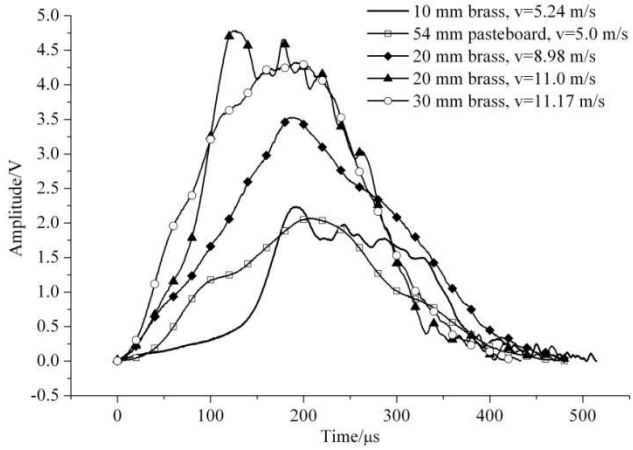


Figure 3 Incident waveforms shaped with different pulse shapers.

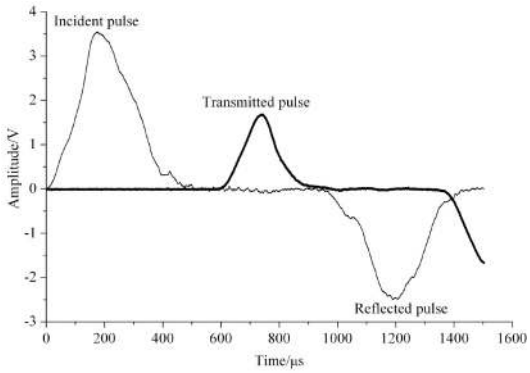


Figure 4 Incident, reflected and transmitted waveforms shaped with a brass pulse shaper ( $\phi 20 \times 1$ mm) for a NAC specimen under the striking velocity of 8.95 m/s.

In the study, various strain-rates were obtained by means of changing projectile's striking velocity. As shown in Figure 5, the relationship between the peak strain-rate $\dot{\varepsilon}_s$ (the strain-rate corresponding to the peak strength) and impact velocity $v$ (m/s) can be approximately linearly expressed as

$$\dot{\varepsilon}_s = A + Bv \tag{1}$$

where parameters $A$ and $B$, together with the standard error $R$, for RAC specimens are summarized in Table 2. It is observed from Figure 5 that at the same striking velocity, the NAC specimens (PC-0) can attain higher peak strain-rate than RAC specimens (RC-25, RC-50, RC-75 and RC-100).

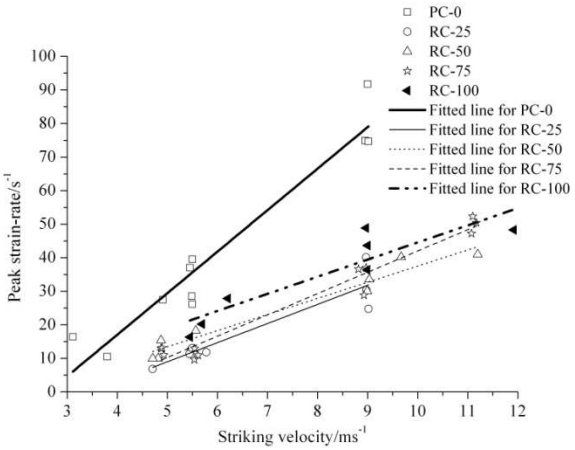


Figure 5 Peak strain-rate versus striking velocity with fitted lines.

Table 2 Parameters in Eq.(1) for RAC specimens.

| | PC-0 | RC-25 | RC-50 | RC-75 | RC-100 |
|---|---|---|---|---|---|
| $A$ | -32.41 | -19.50 | -10.59 | -21.46 | -6.51 |
| $B$ | 12.37 | 5.70 | 4.81 | 6.35 | 5.10 |
| $R$ | 0.92 | 0.84 | 0.95 | 0.96 | 0.78 |

## 3 EXPERIMENTAL RESULTS AND DISCUSSION

### 3.1 Stress versus strain curves and failure patterns

SHPB experiments were conducted at various strain-rates in the range of 10-100 $s^{-1}$. Stress versus strain curves were calculated from signals in the bars with three-wave method, and curves obtained from SHPB tests are shown in Figure 6. The stress increases almost linearly initially and then decreases after the stress achieves the peak value. The strain-rate effect on the peak stress can be seen clearly.

Figure 7 presents the failure patterns of RAC specimens after impact under various striking velocities. It is observed that the failure pattern of RAC specimens is similar with that of NAC specimens. The impact failure becomes more and more violent and decisive with the increase of striking velocity. Under low striking velocity (i.e. <4 m/s), the RAC specimens are failed by the appearance of visible cracks. When the striking velocity is in the range of 4 and 6 m/s, the RAC specimens are failed by the disintegration of the tested cylinders mainly into big pieces. While the striking velocity is further increased, the RAC specimens fractured mainly in very fine fragments.

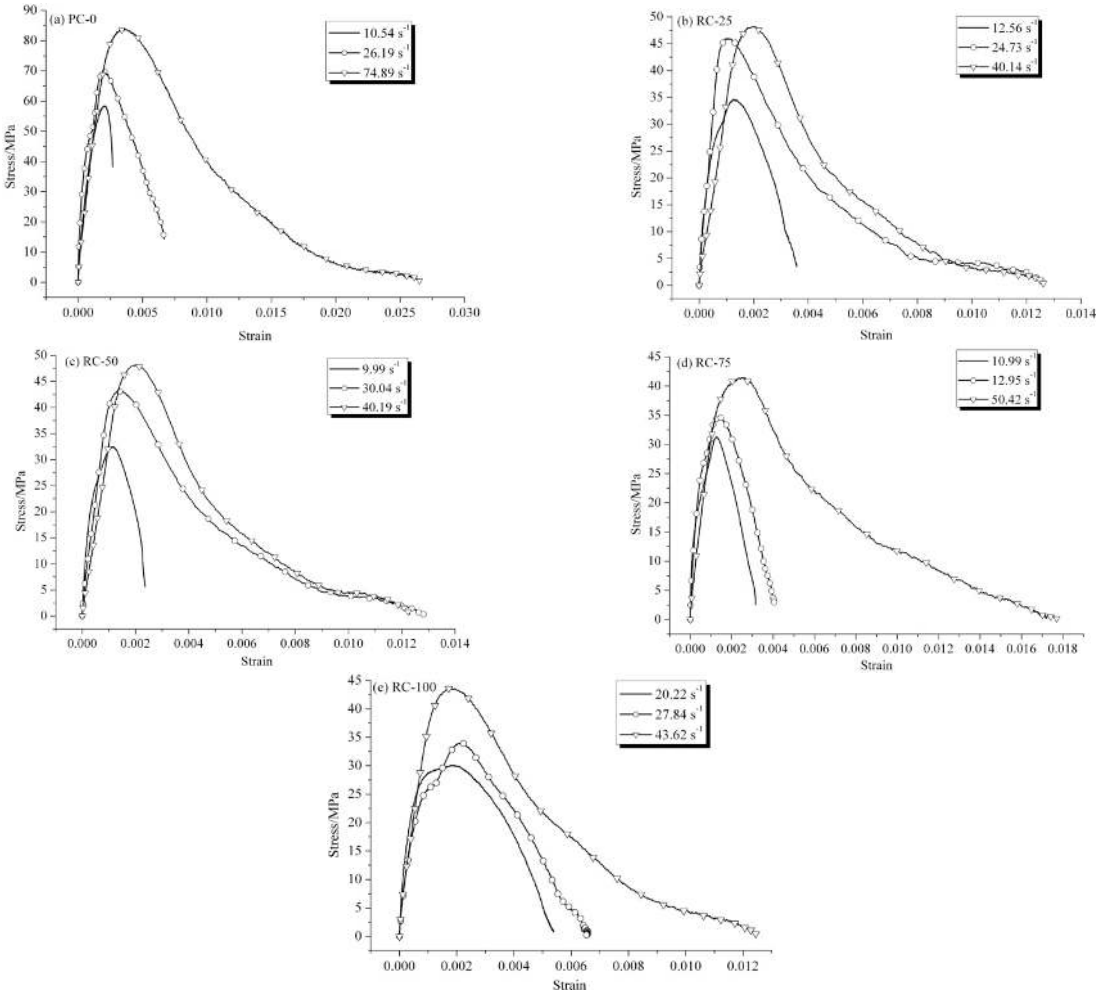


Figure 6 Stress versus strain curves of RAC specimens.




3.1 m/s




4.9 m/s




9.0 m/s

(a) PC-0




4.8 m/s




5.6 m/s




9.7 m/s

(b) RC-50

Figure 7 Failure patterns of RAC specimens under various striking velocities.

### 3.2 Strength

Figure 8(a) shows the dynamic compressive strength $f_{cd}$ versus peak strain-rate for RAC specimens, which indicate that the impact properties of RAC are prominently strain-rate dependent and increase approximately linearly with the increase of peak strain-rate.

It is generally believed that the dynamic increase factor (DIF), which is the ratio of dynamic compressive strength to its corresponding quasi-static value, of concrete is directly depended on the common logarithm of the strain-rate. Therefore, the strain-rate dependence of DIF of RAC at strain-rates in the range of 10-100 $s^{-1}$ can be defined as

$$\mathrm{DIF} = \begin{cases} C + D\log 10(\dot{\varepsilon}_s) & 10^{-5} \le \dot{\varepsilon}_s \le \dot{\varepsilon}_c \mathrm{s}^{-1} \\ E + F\log 10(\dot{\varepsilon}_s) & \dot{\varepsilon}_c \le \dot{\varepsilon}_s \le 100\mathrm{s}^{-1} \end{cases} \tag{2}$$

where the parameter values of $C$, $D$, $E$ and $F$, together with the transition strain-rate $\dot{\varepsilon}_c$ from a low strain-rate sensitivity to a high sensitivity, are summarized in Table 3.

Table 3 Parameters in Eq.(2) for RAC specimens.

| | PC-0 | RC-25 | RC-50 | RC-75 | RC-100 |
|---|---|---|---|---|---|
| $C$ | 1.28 | 1.19 | 1.08 | 1.04 | 1.03 |
| $D$ | 0.054 | 0.037 | 0.014 | 0.0074 | 0.0071 |
| $E$ | 0.23 | 0.65 | 0.37 | 0.73 | -0.25 |
| $F$ | 1.31 | 0.57 | 0.26 | 0.40 | 1.00 |
| $\dot{\varepsilon}_c$ | 6.65 | 10.40 | 11.75 | 6.65 | 19.95 |

Eq.(2), illustrated in Figure 9, clearly indicates that there is a sharp increase in DIF beyond the transition strain-rate of $\dot{\varepsilon}_c$ for RAC specimens, where data points at the strain-rate of $10^{-5}$ $s^{-1}$ are quasi-static compressive strength of RAC specimens, which are summarized in Lu et al. (2013). From Figure 9, it is found that DIF is generally reduced with the increase of RCA replacement ratio. When the testing strain-rate is over the transition strain-rate, the DIF of RAC specimens is largely smaller than that of NAC specimens.

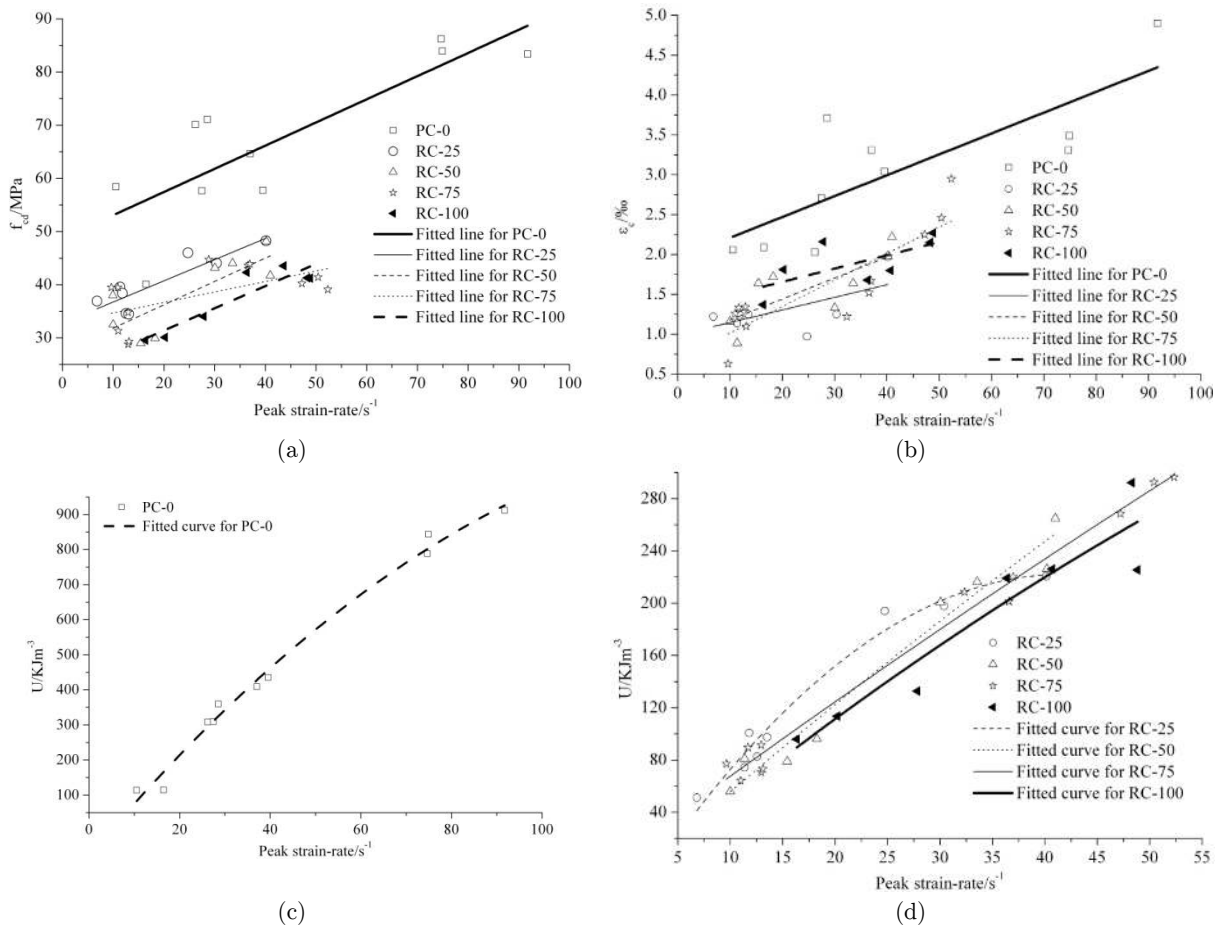


Figure 8 Dynamic compressive strength and critical compressive strain versus peak strain-rate for RAC specimens.

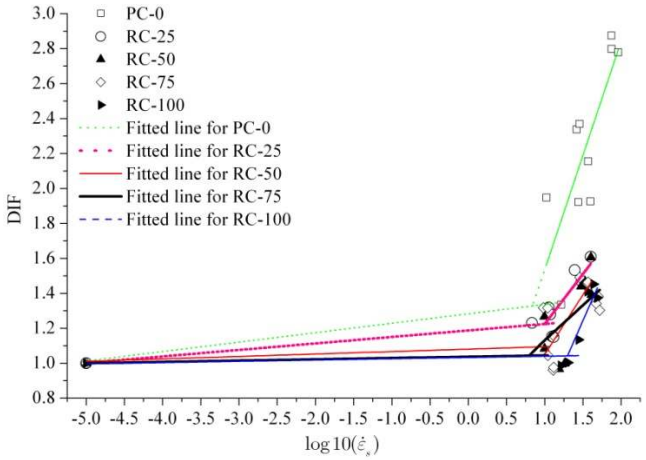


Figure 9 Relationships between DIF and the common logarithm of peak strain-rate for RAC specimens.

### 3.3 Deformation

Critical compressive strain $\varepsilon_c$, which is defined as the stain when the stress reaches the peak, was used to describe the deformation property of RAC specimens. Bischoff et al. (1991) summarized a wide range of concretes of various quasi-static strengths and strain-rates, showing that significant increases in critical compressive strain were sometimes observed during impact loading, although these increases were generally less than those observed for strength. Figure 8(b) depicts a tendency that the critical compressive strain increases with the peak strain-rate, and the critical compressive strain of RAC specimens is generally smaller than that of NAC specimens. The relationship between critical compressive strain and peak strain-rate can be expressed as

$$\varepsilon_c = a + b\dot{\varepsilon}_s \tag{3}$$

in which the parameter values of $a$ and $b$ are summarized in Table 4.

Table 4 Parameters in Eq.(3) for RAC specimens.

| | PC-0 | RC-25 | RC-50 | RC-75 | RC-100 |
|---|---|---|---|---|---|
| $a$ | 1.95 | 0.99 | 0.92 | 0.68 | 1.32 |
| $b$ | 0.026 | 0.016 | 0.026 | 0.033 | 0.017 |

### 3.4 Energy absorption

Specific energy absorption $U$, which is expressed as the energy absorbing per unit volume of material (Yu & Lu, 2005), was used to describe energy absorption property of RAC specimens, and equals to the area of stress-strain curves. As shown in Figure 8(c-d), specific energy absorption is 51.17–911.74 kJ/m$^3$ at peak strain-rate in the range of 10-100 s$^{-1}$, and increases with the increase of peak strain-rate. The relationship between specific energy absorption and peak strain-rate can be expressed as

$$U = c + d\dot{\varepsilon}_s + e\dot{\varepsilon}_s^2 \tag{4}$$

in which the parameter values of $c$, $d$ and $e$ are summarized in Table 5.

In addition, it can be seen in Figure 8(c-d) that the specific energy absorption and its increase velocity of NAC specimens are largely greater than that of RAC specimens. Hence, the efficiency of absorbing impact energy of NAC specimens is higher than that of RAC specimens.

Table 5 Parameters in Eq.(4) for RAC specimens.

| | PC-0 | RC-25 | RC-50 | RC-75 | RC-100 |
|---|---|---|---|---|---|
| $c$ | -72.78 | -36.07 | -14.22 | 8.99 | -14.76 |
| $d$ | 15.29 | 12.35 | 7.13 | 5.93 | 6.74 |
| $e$ | -0.048 | -0.15 | -0.015 | -0.0079 | -0.022 |

## 4 CONCLUSIONS

A 100-mm-diameter SHPB system was used to investigate the dynamic compressive properties of RAC specimens at high strain-rates in the range of 10-100 $s^{-1}$. The main conclusions can be drawn below.

(1)The impact properties of RAC specimens, including dynamic compressive strength, critical compressive strain and specific energy absorption exhibit obvious strain-rate dependency and increase with the increase of peak strain-rate.

(2)The DIF of RAC specimens is generally reduced with the increase of RCA replacement ratio. When the peak strain-rate is over the transition strain-rate, the DIF of RAC specimens is largely smaller than that of NAC specimens.

(3)The critical compressive strain of RAC specimens is generally smaller than that of NAC specimens. Thus, the deformation capacity of RAC specimens is weaker than that of NAC specimens.

(4)The specific energy absorption and its increase velocity of NAC specimens are largely greater than that of RAC specimens. Hence, the energy absorption capacity of RAC specimens is lower than that of NAC specimens.

### Acknowledgements

First author would like to acknowledge the sponsor by the Scientific Research Foundation for the Returned Overseas Chinese Scholars, State Education Ministry (13zs1101).

### References

Bischoff, P.H. and Perry, S.H. (1991). Compressive behaviour of concrete at high strain rates. Materials and Structures 24: 425-450.

Chakradhara Rao, M., Bhattacharyya, S.K. and Barai, S.V. (2011). Behaviour of recycled aggregate concrete under drop weight impact load. Construction and Building Materials 25: 69-80.

Li, W.M. and Xu, J.Y. (2009). Mechanical properties of basalt fiber reinforced geopolymeric concrete under impact loading. Materials Science and Engineering A 505: 178-186.

Lu, Y.B. and Li, Q.M. (2010). Appraisal of pulse shaping technique in split Hopkinson pressure bar tests for brittle materials. International Journal of Protective Structures 1: 363-390.

Lu, Y.B., Chen, X., Teng, X. and Zhang, S. (2013). Experimental study on quasi-static compressive mechanical performance of recycling concrete. Journal of Southwest University of Science and Technology (Natural Science Edition), 2013 (in Press).

Ravichandran, G. and Subhash, G. (1994). Critical appraisal of limiting strain rates for compression testing of ceramics in a split Hopkinson pressure bar. Journal of the American Ceramic Society 77: 263-267.

Rong, Z.D., Sun, W. and Zhang, Y.S. (2010). Dynamic compression behavior of ultra-high performance cement based composites. International Journal of Impact Engineering 37: 515-520.

Wang, Z.L., Liu, Y.S. and Shen, R.F. (2008). Stress–strain relationship of steel fiber-reinforced concrete under dynamic compression. Construction and Building Materials 22: 811-819.

Yu, T.X. and Lu, G.X. (2005). Energy Absorption of Structures and Materials. Chemical Industry Press, Beijing (in Chinese).